Dalton Transactions

PAPER

View Article Online
View Journal | View Issue

Cite this: *Dalton Trans.*, 2014, **43**, 13649

New Pt^{II} diimine–dithiolate complexes containing a 1,2-dithiolate-1,2-*closo*-dicarbadodecarborane: an experimental and theoretical investigation†

Anna Pintus,[a] M. Carla Aragoni,[a] Simon J. Coles,[b] Susanne L. Coles (née Huth),[b] Francesco Isaia,[a] Vito Lippolis,[a] Ana-Daniela Musteti,[c] Francesc Teixidor,[c] Clara Viñas[c] and Massimiliano Arca*[a]

Received 26th June 2014,
Accepted 12th July 2014

DOI: 10.1039/c4dt01929f

www.rsc.org/dalton

Five new [Pt(N^N)(dtoc)] complexes (**1–5**; N^N = diimine: 2,2′-bipyridine and its 4,4′-alkyl/aryl-substituted derivatives or 1,10-phenanthroline; $dtoc^{2-}$ = 1,2-dithiolate-1,2-*closo*-dicarbadodecaborane) have been synthesized and characterized by spectroscopic and electrochemical methods, and by means of X-ray diffraction in the case of complexes **1** and **4**. Hybrid DFT and time-dependent (TD) DFT calculations were performed on complexes **1–5** and the previously reported complex [Pt(Ph_2phen)(dtoc)] (**6**; Ph_2phen = 4,7-diphenyl-1,10-phenanthroline) both in the gas phase and in the presence of several solvents (CH_2Cl_2, $CHCl_3$, CH_3CN, acetone, THF, DMF, DMSO, and toluene) to gain an insight into the electronic structure of the complexes and explain their experimental features. Theoretical calculations allowed for the determination of structure–property relationships within the series of the six complexes considered, and the prediction of their second order nonlinear optical (SONLO) properties by evaluating their first static hyperpolarizabilities (β_{tot}).

Introduction

Since the first reports by Miller and Dance in 1973,[1] diimine–dithiolate metal complexes [M(N^N)(S^S)] have received a great deal of attention. These systems have been, in fact, applied to second order nonlinear optics (SONLO),[2,3] dye-sensitized solar cells,[4–8] light-to-chemical energy conversion,[9,10] DNA intercalation,[11,12] and as conducting[13] and magnetic[14] materials or sensors.[15] Such a variety of potential applications arise from their peculiar electronic features. In fact, [M(N^N)(S^S)] complexes undergo reversible electrochemical processes[16] and show large molecular hyperpolarizabilities,[17] room-temperature luminescence in solution,[18,19] and a peculiar intense (molar extinction coefficient ε up to 10^4 M^{-1} cm^{-1}) solvatochromic absorption in the vis-NIR region.[20,21] This absorption, thoroughly investigated in the past by both experimental and theoretical means,[22] was assigned to a charge-transfer (CT) transition occurring from the HOMO, mainly localized on the S^S ligand and partly on the central metal ion, to the LUMO, centred on the diimine N^N.[23] The nature of this transition, often described as a mixed-metal/ligand-to-ligand charge-transfer (MMLL'CT),[24] accounts for the negative solvatochromism featured by the corresponding absorption, since it generates an excited state, which is less polar or polarized in the opposite direction with respect to the ground state.[25]

Starting from the pioneering work carried out by Eisenberg and co-workers in the 1990s,[26,27] a large number of diimine–dithiolate complexes have been reported, mainly featuring Pt^{II} as a central metal ion. The possibility of tuning both the electrochemical and photophysical properties of these chromophores by systematically varying both the central metal ion[28] and the S^S and N^N ligand[29] was distinctly proved. In this context, some of the authors recently reported on a series of new Pt^{II} diimine–dithiolate complexes featuring differently functionalized 1,2-dithiolato ligands belonging to the classes of R-edt^{2-} (monosubstituted ethylene-1,2-dithiolates; R = phenyl, 2-naphtyl, 1-pyrenyl)[30,31] and R-$dmet^{2-}$ (*N*-substituted

[a]*Dipartimento di Scienze Chimiche e Geologiche, Università degli Studi di Cagliari, S.S. 554 bivio per Sestu, 09042 Monserrato, CA, Italy. E-mail: marca@unica.it*
[b]*Department of Chemistry, Faculty of Natural and Environmental Sciences, University of Southampton, Highfield, Southampton SO17 1BJ, UK*
[c]*Institut de Ciència de Materials de Barcelona (ICMAB-CSIC), Campus UAB, 08193 Bellaterra, Spain*

† Electronic supplementary information (ESI) available: Details on the characterization of complexes **2–5**, crystallographic data for complexes **1** and **4**, metric parameters optimized in the gas phase and in selected solvents, calculated eigenvalues and MO compositions, NPA charges, details on vertical transitions calculated at the TD-DFT level, correlations between UV–vis absorption wavelengths in selected solvents and empirical parameters, correlation between CV data and UV–vis absorption wavelengths, KS-MO scheme calculated for complex **2** in DMSO, correlation between experimental and calculated absorption wavelengths in DMSO, correlation between experimental and calculated solvatochromic absorption wavelengths. CCDC 1010434 and 1010435. For ESI and crystallographic data in CIF or other electronic format see DOI: 10.1039/c4dt01929f

2-thioxo-1,3-thiazoline-4,5-dithiolates; R = methyl, ethyl, phenyl),[32,33] along with variously alkyl- and aryl-substituted 2,2′-bipyridine and 1,10-phenanthroline ligands, thus showing the possibility of fine-tuning the linear and nonlinear optical properties of these systems.[34]

The twelve-vertex 1,2-*closo*-$C_2B_{10}H_{12}$ icosahedral carborane has been widely studied.[35] The unique stabilities and geometrical properties of the isomeric *closo* $C_2B_{10}H_{12}$ carboranes suggested this species as a building block for stereo precise structural platforms with novel reaction centres having properties that cannot be achieved with organic hydrocarbon compounds.[36] In addition, the 1,2-*closo*-$C_2B_{10}H_{12}$ cluster is electron-withdrawing through the carbon atoms[37] and electron donating through the boron atoms. Consequently, when sulphur atoms are bonded to the carbon cluster atoms, as in the dithiol 1,2-$(SH)_2$-*closo*-$C_2B_{10}H_{10}$ (H_2dtoc), the electron density will be depleted on them, thus varying the potentials required for the electrochemical reduction of the corresponding complexes.[38] In particular, as far as diimine–dithiolate systems are concerned, it is reasonable to assume that more strong electron-deficient[39] moieties such as the 1,2-*closo*-$C_2B_{10}H_{12}$ cluster could affect the electrochemical and optical properties of these complexes with respect to those obtained with organic dithiolates.

In this context, we report on the synthesis, characterization and DFT investigation of five new [Pt(N^N)(S^S)] complexes featuring the 1,2-dithiolato-1,2-*closo*-dicarbadodecaborane ligand ($dtoc^{2-}$),[40] in combination with differently substituted 2,2′-bipyridine and 1,10-phenanthroline derivatives. The properties of the newly synthesized complexes were compared with those based on organic ethylene-1,2-dithiolates[30–33] and with [Pt(Ph_2phen)(dtoc)] (Ph_2phen = 4,7-diphenyl-1,10-phenanthroline), the only example of a [Pt(N^N)(S^S)] complex featuring the $dtoc^{2-}$ ligand reported so far.[41–43]

Results and discussion

Synthesis

In the present study, five new complexes belonging to the general class [Pt(N^N)(dtoc)] were synthesized following the general preparation method for [Pt(N^N)(S^S)] systems,[1] which exploits the reaction of the desired S^S dithiolato ligand with a metal precursor of the type [$PtCl_2$(N^N)] (Scheme 1).[44,45] In particular, the diimines N^N = 2,2′-bipyridine (bipy), 1,10-phenanthroline (phen), 4,4′-dimethyl-2,2′-bipyridine (Me_2bipy), 4,4′-di(*tert*-butyl)-2,2′-bipyridine (tBu_2bipy), and 4,4′-diphenyl-2,2′-bipyridine (Ph_2bipy) were employed for the synthesis of the corresponding [$PtCl_2$(N^N)] complexes, which were reacted with the 1,2-dithiolate-1,2-*closo*-dicarbadodecarborane ligand (generated *in situ* by the deprotonation of the corresponding dithiol H_2dtoc)[35b] to afford the desired [Pt(N^N)(dtoc)] complexes **1–5**.

Crystallographic studies

X-ray diffraction quality single crystals were successfully grown for complexes **1** and **4** (Fig. 1 and Table S1 in ESI†). The platinum atom is coordinated in both complexes by the two diimine N atoms and the two S atoms of the $dtoc^{2-}$ ligand in a distorted square planar *cis*-"S_2N_2" configuration. The Pt–N and Pt–S bond lengths closely resemble the values found in two similar bis-monothiolato *o*-carborane platinum complexes containing 2,2′-bipiridine[46] and substituted 1,10-phenantroline ligands,[41,43] and are in the range of bond lengths typical for

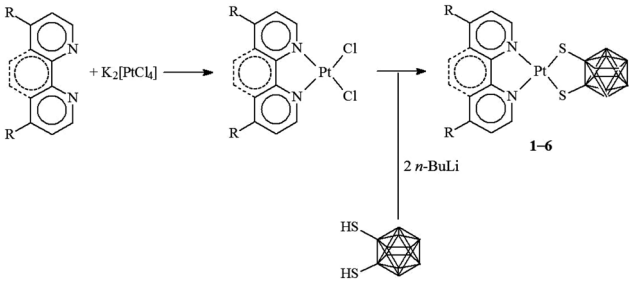

Scheme 1 General pathway for the synthesis of [Pt(N^N)(dtoc)] complexes **1–6**. N^N = bipy (**1**), phen (**2**), Me_2bipy (**3**), tBu_2bipy (**4**), Ph_2bipy (**5**), and Ph_2phen (**6**).

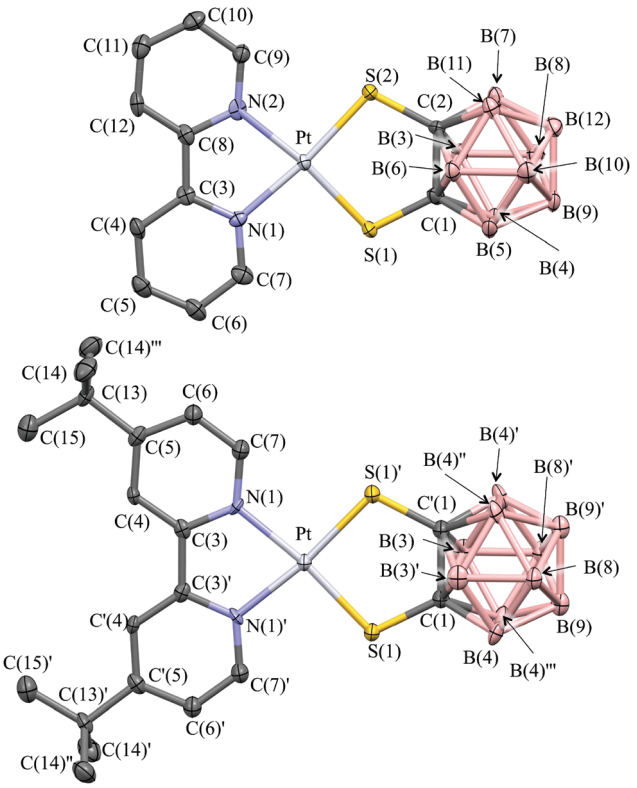

Fig. 1 ORTEP drawing of complexes **1** (top) and **4** (bottom) showing the atom-labeling scheme. Thermal ellipsoids are drawn at the 60% probability level. Hydrogen atoms have been omitted for clarity. For complex **1**: Pt–S(1) 2.2725(17), Pt–S(2) 2.2789(16), Pt–N(1) 2.057(6), Pt–N(2) 2.055(6), S(1)–C(1) 1.777(7), S(2)–C(2) 1.790(7), C(1)–C(2) 1.638(9) Å; S(1)–Pt–S(2) 92.35(6), N(1)–Pt–N(2) 79.8(2), N(1)–Pt–S(2)–C(2) 174(2)°. For complex **4**: Pt–S(1) 2.2686(4), Pt–N(1) 2.046(4), S(1)–C(1) 1.796(5), C(1)–C(1)′ 1.631(10) Å; S(1)–Pt–S(1)′ 92.19(7), N(1)–Pt–N(1)′ 78.6(2)°. ′ = 1 − *x*, 1/2 − *y*, *z*.

other Pt^{II} diimine–dithiolate systems structurally characterized so far [2.045(16) and 2.239(16) Å, respectively].[47]

Analogously, C–S and C–C bond lengths within the $dtoc^{2-}$ ligand in complexes **1** and **4** are very close to the mean values found in the Cambridge Structural Database (CSD) for complexes featuring $dtoc^{2-}$ as a bidentate ligand coordinated to a single transition metal ion [1.782(9) and 1.652(20) Å, respectively],[48] and only slightly different from the $C_{carborane}$–thiol and the skeletal C–C bond distances found in the carboranyl sulphide anion $[1,2\text{-}S(Ph)C_2B_{10}H_{10}]^-$.[49] The dithiol-*o*-carborane forms in both cases a five membered chelate ring, with S–Pt–S/N–Pt–N angles of 92.35(6)/79.8(2) and 92.19(7)°/78.6(2)° for complexes **1** and **4**, respectively, which fall within the expected ranges.[50]

In complex **4** the bipyridyl ligand lies in the PtN_2S_2 coordination plane, and a mirror plane bisects the molecule by passing through the bond joining the two pyridine rings, the platinum ion, and the C–C bond of carborane. Complex **1** displays a similar arrangement of the bipyridyl ligand, which however slightly deviates from planarity [dihedral angle N(1)–Pt–S(2)–C(2) = 173.92°; Fig. 1]. Both complexes **1** and **4** are packed in a head-to-tail fashion to form columnar structures along axis *a* and *b* respectively, but they differ in the nature of the interactions involved. In complex **1** short intermolecular Pt···C contacts align the complex molecules in pillars developing along the direction of the *a*-axis with alternating Pt···C distances of 3.395(8) and 3.530(8) Å (Fig. 2).[51] Similar short contacts have been explained with a weak axial interaction between the filled d_{z^2} orbital of platinum and the π* antibonding orbital of the involved C atoms in the bipyridyl ring.[52] Weak intermolecular interactions involving the B atoms of the $dtoc^{2-}$ ligand and the H atoms of both ligands hold the stacks together [B(6)···H(11) 3.180, B(10)···H(7A) 3.163, B(7)···H(6) 2.884, B(3)···H(6) 3.179, B(2)···H(6) 3.039, B(9)···H(11) 3.134 Å].

In complex **4** the molecules are aligned into mono-dimensional columns running along the crystallographic *a*-axis through extensive face-to-face π–π interactions involving both rings of bipy moieties with stacking distances of 3.89 Å, though no interactions involving the platinum ions can be evidenced. Weak interactions involving the H atoms of the *tert*-butyl substituents of the 2,2′-bipyridines and the B atoms of the $dtoc^{2-}$ ligand [B(1)···H(14B) 3.034, B(3)···H(14B) 3.138, B(4)···H(14B) 3.137 Å] are responsible for the 3D packing of the columns. It is noteworthy, probably due to the bulky substituents at the pyridine rings, that the structure of **4** contains solvent accessible channels running along the *b*-axis (376.16 $Å^3$, 12.6% of the cell volume, Fig. 3).[53]

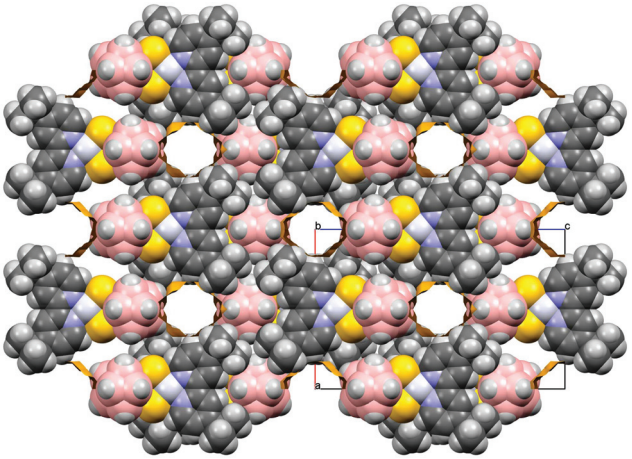

Fig. 3 Space fill style view evidencing the void channels in the packing of complex **4**.

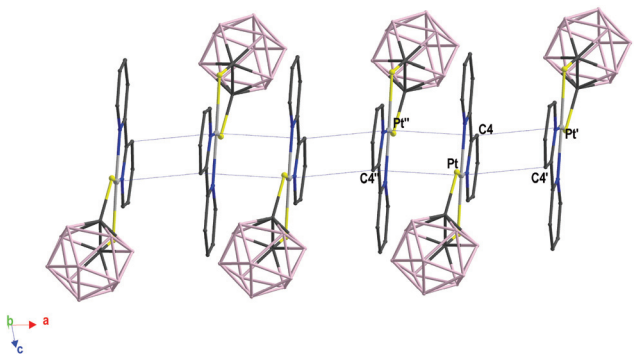

Fig. 2 Packing views of the columnar arrangement in complex **1**. Alternate short and long contacts in complex **1**: Pt···C4′ 3.395(8), Pt···C4″ 3.530(8) Å (′ 2 − *x*, 1 − *y*, −*z*; ″ 1 − *x*, 1 − *y*, −*z*). Hydrogen atoms have been omitted for clarity.

Electrochemistry

Cyclic voltammetry (CV) measurements (Table 1) performed in dry DMSO showed that complexes **1–6** feature monoelectronic reversible (i^I_{pc}/i^I_{pa} values in the range 0.8–1.3) reduction processes ($E^I_{1/2}$) between −1.709 and −1.536 V *vs.* Fc^+/Fc (Fig. 4 for complex **1**), corresponding to the reduction of the neutral species to the corresponding monoanions. The potential values $E^I_{1/2}$ determined for complexes **1–6** can be compared with the first reduction potentials determined for the [Pt(N^N)(Me-dmet)] complexes featuring the same diimine ligands under the same experimental conditions.[34,54] In fact, the two sets of data are very similar and linearly correlated (R^2 = 0.95). On passing from S^S = $Me\text{-}dmet^{2-}$ to $dtoc^{2-}$, the potentials are only slightly shifted (on an average by 0.018 V), confirming that the potential of this reduction process depends on the nature of the diimine.

Table 1 Electrochemical data recorded by CV for complexes **1–6** in DMSO solution at 298 K (potentials *E* in V)[a]

	$E^I_{1/2}$	$\lvert E^I_{pc}-E^I_{pa}\rvert$	i^I_{pc}/i^I_{pa}	$E^{II}_{1/2}$	$\lvert E^{II}_{pc}-E^{II}_{pa}\rvert$	i^{II}_{pc}/i^{II}_{pa}
1	−1.593	0.088	1.0	−2.251	0.100	1.1
2	−1.604	0.081	1.3	−2.229	0.047	1.2
3	−1.709	0.135	0.8	—	—	—
4	−1.698	0.044	1.1	—	—	—
5	−1.536	0.071	1.0	−2.090	0.091	0.4
6	−1.541	0.071	1.1	−2.100	0.091	0.9

[a] All potentials $E_{1/2}$, E_{pc}, and E_{pa} are referred to the Fc^+/Fc couple. Scan rate 100 mV s^{-1}.

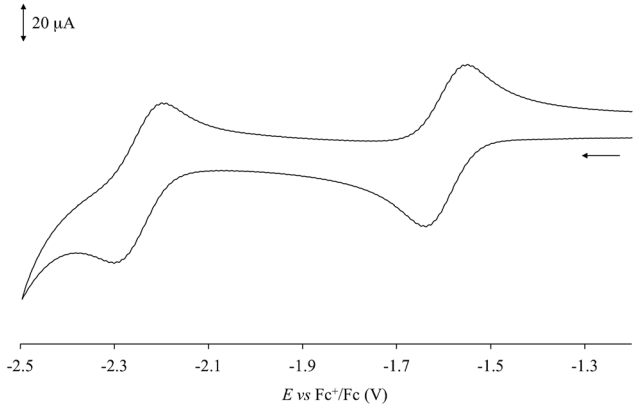

Fig. 4 Cyclic voltammogram recorded at a platinum electrode in an anhydrous DMSO solution of **1** [298 K; scan rate 100 mV s^{-1}; supporting electrolyte $[NBu_4][PF_6]$ 0.1 M].

Complexes **1**, **2**, **5**, and **6** exhibit a further *quasi*-reversible reduction (i^{II}_{pc}/i^{II}_{pa} = 0.4–1.2) at about −2.1/−2.2 V *vs.* Fc^+/Fc ($E^{II}_{1/2}$, Table 1 and Fig. 4 for complex **1**), which leads from monoanionic to dianionic species. The second reduction process was previously reported for [Pt(Ph_2Phen)(dtoc)] (**6**; Ph_2Phen = 4,7-diphenyl-1,10-phenanthroline; Scheme 1) in DMF ($E_{1/2}$ = −2.14 V *vs.* Fc^+/Fc).[43] Weinstein and co-authors supposed this process to be localized on the diimine,[43] although in analogy to what was reported for different [Pt(bipy)L_2] (L = py, Me_2N-py, Cl), [Pt(bipy)(en)], and [Pt(phen)$(py)_2$] complexes,[55] this reduction could be attributed to the formation of a dianionic Pt^I radical species $[Pt^I(N\hat{}N^{\bullet})(S\hat{}S)]^{2-}$.[56]

An examination of the reduction potentials $E^{I}_{1/2}$ and $E^{II}_{1/2}$ listed in Table 1 shows that no significant effect is observed on passing from N^N = bipy to N^N = phen in complexes **1** and **2**, respectively. The introduction of alkyl substituents at the diimine (**3** and **4**) induces a potential shift towards more negative values, while phenyl substituents (**5** and **6**) shift both $E^{I}_{1/2}$ and $E^{II}_{1/2}$ towards more positive values with respect to the complexes **1** and **2** featuring unsubstituted diimines. Given the predominant localization of the LUMO on the diimine in [Pt(N^N)(S^S)] systems,[23] this trend suggests that aryl substituents at the N^N ligands induce a stabilization of the LUMO, while alkyl substituents cause an opposite effect.[34] This could also account for the absence of the reduction to dianionic forms in the case of complexes **3** and **4**, whose $E^{II}_{1/2}$ potential would be too negative to be electrochemically explored.

Although a further oxidation process at about 0.95 V *vs.* the Fc^+/Fc couple was reported in DMF for **6**,[43] this process was not observed in DMSO within the explored potential range. The lack of oxidation processes to cationic species suggests a remarkable stabilization of the HOMO in **1–6** as compared to different diimine–dithiolate complexes, possibly ascribed to the electron-withdrawing effect of the 1,2-*closo*-$C_2B_{10}H_{12}$ cluster.[38]

Absorption UV–vis spectroscopy

Diimine–dithiolate complexes show a peculiar low-energy solvatochromic absorption in the visible region.[20] Accordingly, the UV-vis absorption spectra recorded in DMSO for complexes **1** and **3–5**, bearing bipyridine ligands, feature a broad and asymmetric absorption band in the visible region, with absorption maxima in the range 420–440 nm, and molar extinction coefficients ε between 4700 and 8200 M^{-1} cm^{-1} (Table 2 and Fig. 5 for complex **1**). In the case of complexes **2** and **6**, bearing 1,10-phenanthroline ligands, this absorption is split into two bands, falling at 378/395 and 427/441 nm, respectively (ε values of about 6000–7000 M^{-1} cm^{-1} in DMSO; Table 2 and Fig. 5 for complex **2**), in agreement with the data previously reported for complex **6**.[43] An examination of the absorption spectra recorded for complexes **1–6** in eight different solvents (namely CH_2Cl_2, $CHCl_3$, CH_3CN, acetone, THF, DMF, DMSO, and toluene) shows a remarkable solvatochromism for the absorption bands in the visible region, with a shift in the λ_{max} value of about 40–60 nm.

In particular, both the broad absorption featured by the bipyridine-containing complexes and the two bands shown in the case of complexes **2** and **6** display a negative solvatochromism, and a dependence of their ε values on the nature of the solvent (Table 2 and Fig. 6 for complex **2**).

The observed solvatochromic behaviour is in agreement with the empirical scale previously proposed by Eisenberg and co-workers for platinum diimine–dithiolate complexes,[20] thus suggesting a CT character for the electronic transitions involved (Fig. S1† for complex **2**).

The λ_{max} values recorded in DMSO for the solvatochromic absorption at the lowest energy of complexes **1–6** strongly depend on the nature of the diimine, analogously to what was previously observed for [Pt(N^N)(S^S)] complexes featuring

Table 2 Absorption maxima λ_{max} (in nm) and molar extinction coefficients (in M^{-1} cm^{-1}, in parentheses)[a] of the lowest energy solvatochromic absorption band in the Vis region for complexes **1–6** in different solvents

	CH_2Cl_2	$CHCl_3$	CH_3CN	Acetone	THF	DMF	DMSO	Toluene
1	447 (6300)	452 (6500)	425 (5700)	434 (5600)	452 (6300)	428 (5800)	424 (5800)	481
2	444 (6200)	453 (6600)	426 (4400)	436 (5800)	453 (6100)	430 (6000)	427 (6100)	476
3	437 (5200)	434 (4300)	445	428 (5000)	445 (4900)	425 (4400)	420 (4700)	454
4	438 (7300)	447 (7200)	418 (6700)	428 (7200)	446 (7600)	423 (6700)	419 (6000)	470 (8600)
5	458 (9300)	467 (7000)	438 (8900)	448 (8100)	466 (7700)	444 (8400)	439 (8200)	492
6	452 (8000)	460 (8200)	438 (7300)	448 (8700)	463 (8400)	444 (7000)	441 (6700)	484 (8000)

[a] If not reported, the molar extinction coefficients were not determined for solubility reasons.

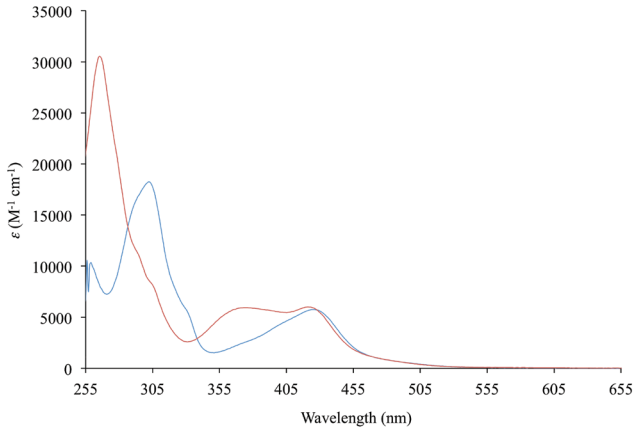

Fig. 5 UV–vis absorption spectra (255–655 nm) recorded for complexes **1** (blue line) and **2** (red line) in DMSO.

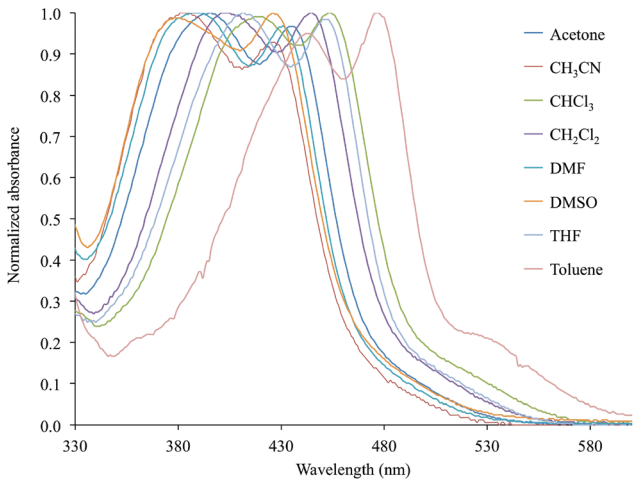

Fig. 6 Normalized absorption spectra in the Vis region (330–600 nm) recorded for complex **2** in eight selected solvents (Table 2).

R-dmet^{2-} 1,2-dithiolato ligands.[34] In particular on passing from complexes **1** and **2**, bearing unsubstituted diimines, to complexes **5** and **6**, where the N^N ligands are phenyl-substituted, a red-shift can be observed. On the other hand, alkyl substituents (complexes **3** and **4**) induce a blue-shift of the λ_{max} value of the corresponding complexes. Since the solvatochromic band is attributed to the HOMO–LUMO transition, its wavelength can be correlated to the LUMO energy, and thus spectroscopic and electrochemical CV data have been cross-compared. In fact, a linear correlation holds between the λ_{max} values and the $E_{1/2}$ potentials (Fig. 7 and S2† for $E^{I}_{1/2}$ and $E^{II}_{1/2}$, respectively; R^2 = 0.82 and 0.98). This correlation suggests that the variation of the λ_{max} values should be attributed mainly to a variation in the energies of the LUMO, localized in the diimine, while the uppermost filled MOs would not be affected, and should therefore be localized on the dtoc^{2-} ligand and/or the central metal ion, in agreement with what was reported for different [Pt(N^N)(S^S)] complexes.[25]

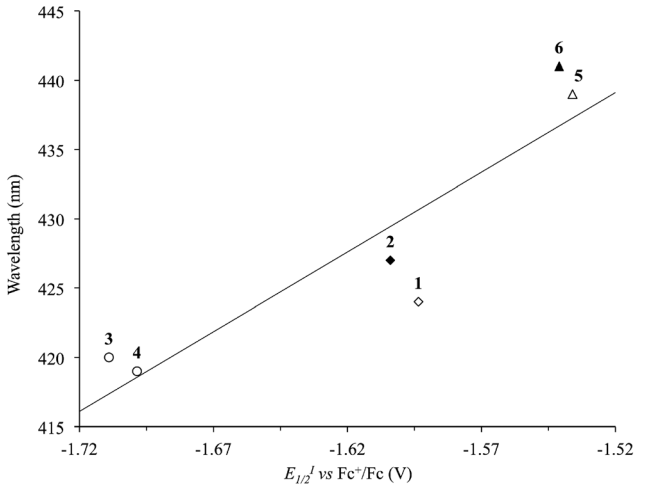

Fig. 7 Correlation between the reduction potentials $E^{I}_{1/2}$ (V *vs.* Fc$^+$/Fc) and the λ_{max} of the solvatochromic absorption (nm) in DMSO solutions of complexes **1–6** (R^2 = 0.82; Tables 1 and 2). N^N = unsubstituted (rhombs) 2,2′-bipyridine (empty) or 1,10-phenathroline (filled), and alkyl (circles) or phenyl (triangles) derivatives.

Theoretical calculations

With the aim of gaining an insight into the electronic structure of the title complexes and interpreting the electrochemical and spectroscopic features observed experimentally, a theoretical investigation was performed on complexes **1–6** at the density functional theory (DFT) level.[57] Following the good results previously obtained with different [Pt(N^N)(S^S)] complexes,[34] the hybrid PBE0 functional was adopted,[58] and the all-electron double-ζ basis sets (BSs) with polarization functions by Schäfer, Horn, and Ahlrichs[59] were exploited for light atomic species. For the heavier Pt species, the CRENBL BS[60] with relativistic effective core potentials (RECPs)[61,62] was chosen to account for the relativistic effects occurring in the case of third-row transition metal ions.[63] Given the role played by the solvent in the spectroscopic features of Pt^{II} diimine–dithiolate complexes, solvation calculations were also carried out at the same level of theory using the integral equation formalism of the polarizable continuous model (IEF-PCM) within the self-consistent reaction field (SCRF) approach.[64] Calculations were performed both in the gas phase and in the presence of DMSO for all the complexes **1–6**, and in the case of complex **1**, solvation calculations were performed by considering all of the eight solvents employed for the spectroscopic measurements (see above; Table S2†).

The structural features optimized both in the gas phase and in DMSO are summarized in Table 3. Very similar sets of data were found for the optimized geometries of complexes **1–6** in the gas phase, the Pt–S and Pt–N distances falling in the ranges 2.284–2.289 and 2.050–2.059 Å, respectively.

For all the complexes, almost no changes in the optimized bond distances and angles were observed upon considering solvation in the calculations, the principal bond distances and angles varying by less than 0.1 Å and 1°, respectively. The most significant difference regards the N(1)–Pt–S(2)–C(2) dihedral

Table 3 Selected optimized bond lengths (in Å) and angles (in °) for complexes **1–6** in the gas phase and in DMSO (IEF-PCM SCRF model, in parentheses)[a]

	1	2	3	4	5	6
Pt–S(1)	2.287 (2.305)	2.284 (2.302)	2.289 (2.306)	2.289 (2.306)	2.288 (2.306)	2.286 (2.303)
Pt–S(2)	2.287 (2.305)	2.284 (2.302)	2.289 (2.306)	2.289 (2.306)	2.288 (2.306)	2.286 (2.303)
Pt–N(1)	2.053 (2.052)	2.059 (2.059)	2.053 (2.051)	2.052 (2.051)	2.050 (2.050)	2.054 (2.053)
Pt–N(2)	2.053 (2.052)	2.059 (2.059)	2.053 (2.051)	2.052 (2.051)	2.050 (2.050)	2.054 (2.053)
S(1)–C(1)	1.795 (1.793)	1.795 (1.794)	1.795 (1.793)	1.795 (1.793)	1.795 (1.793)	1.795 (1.794)
S(2)–C(2)	1.795 (1.793)	1.795 (1.794)	1.795 (1.793)	1.795 (1.793)	1.795 (1.793)	1.795 (1.794)
C(1)–C(2)	1.617 (1.621)	1.618 (1.622)	1.618 (1.623)	1.618 (1.624)	1.618 (1.623)	1.619 (1.624)
S(1)–Pt–S(2)	90.36 (90.31)	90.99 (90.72)	90.39 (90.26)	90.46 (90.22)	90.47 (90.17)	90.89 (90.59)
N(1)–Pt–N(2)	79.22 (79.49)	80.08 (80.30)	79.10 (79.31)	80.00 (79.37)	79.11 (79.34)	79.64 (79.82)
N(1)–Pt–S(2)–C(2)	170.88 (175.31)	169.37 (174.10)	170.09 (174.01)	169.87 (174.93)	170.04 (175.19)	169.78 (174.97)

[a] Atom labelling scheme as reported in Fig. 1 for complex **1**.

angle, which is increased for all complexes by about 5° towards planarity on passing from the gas phase to the implicitly solvated species. The calculations performed in the case of complex **1** taking into account eight different solvents confirm that the optimized parameters vary only slightly upon changing the solvent (Table S2†).[65] A very good agreement was found between the parameters optimized in the gas phase and the corresponding experimental structural data for complexes **1** and **4**, with all of the bond lengths and angles differing by less than 0.03 Å and 2°, respectively.

In Fig. 8 and S3† the ground-state (GS) bonding scheme is shown in terms of the frontier Kohn–Sham (KS) molecular orbital (MO) scheme for complexes **1** and **2**, respectively. Analogously to what was reported for related complexes,[66,67] KS-HOMO and KS-HOMO−1 (MOs 102 and 101, respectively, in Fig. 8) are π-in-nature MOs mainly localized on the sulphur atoms of the $dtoc^{2-}$ ligand. The stabilization effect induced by the electron-withdrawing $dtoc^{2-}$ ligand allows for a larger extent of mixing between the ligand fragment molecular orbitals (FMOs) and the atomic orbitals (AOs) of the metal ion in the title complexes. In fact, KS-HOMOs show a remarkable contribution from 5d AOs of the Pt atom, which increases when the solvent is taken into account (17–18 and 24–25% in the gas phase and in DMSO, respectively; Fig. 9 for complex **1**). Accordingly, KS-HOMO eigenvalues calculated for complexes **1–6** in the gas phase[68] are remarkably more negative than those calculated at the same level of theory for different [Pt(N^N)(S^S)] complexes reported previously.[34,69] The stabilization of the eigenvalues calculated for HOMOs and HOMO−1s for the complexes featuring the $dtoc^{2-}$ ligand is reflected in the absence of oxidation processes in the voltammograms recorded for complexes **1–6** in DMSO solution (see above).

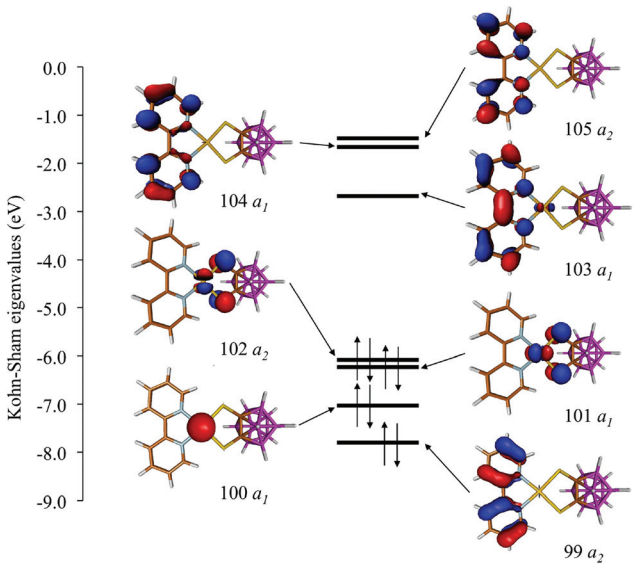

Fig. 8 KS-MO scheme and isosurface drawings calculated for complex **1** in DMSO (IEF-PCM SCRF model; C_s point group; contour value = 0.05 *e*).

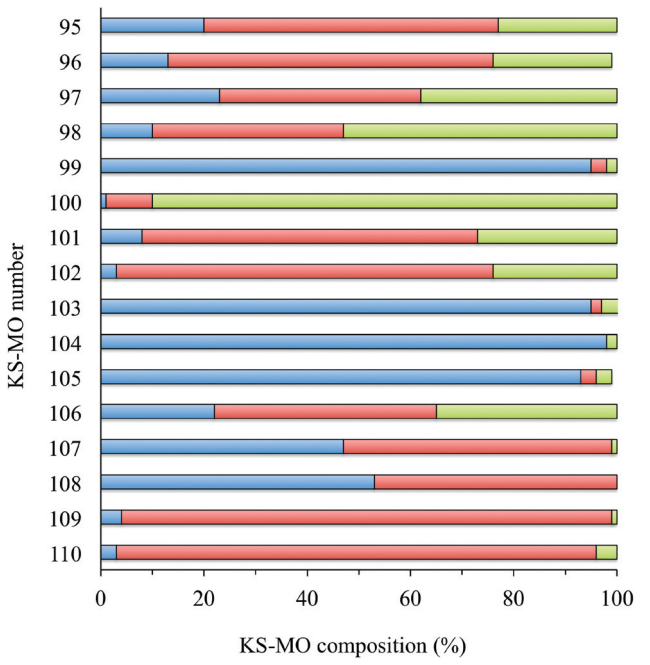

Fig. 9 Frontier molecular orbital (KS-MOs 95–105; KS-HOMO = 102, KS-LUMO = 103) composition calculated for complex **1** in DMSO [fragments: platinum atom, green; $dtoc^{2-}$ ligand, red; N^N ligand (blue)].

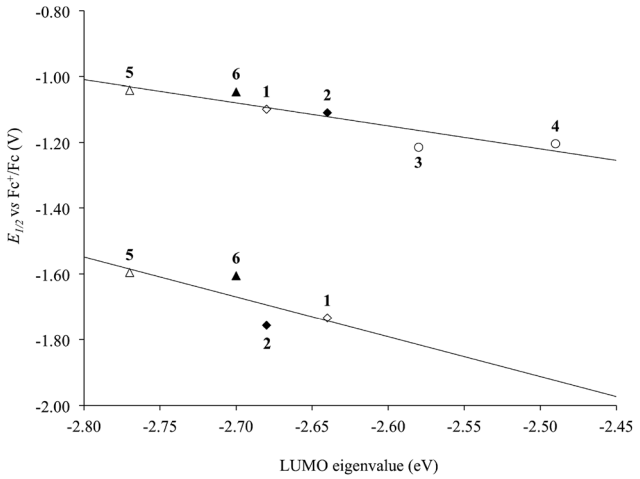

Fig. 10 Correlation between the experimental half-wave potentials of the $E^{I}_{1/2}$ (top) and $E^{II}_{1/2}$ (bottom) reduction processes (V *vs.* Fc^+/Fc) and the IEF-PCM TD-DFT calculated KS-LUMO eigenvalues (eV) for complexes **1–6** in DMSO (R^2 = 0.84 and 0.61, respectively; Tables 1 and S3†). N^N = unsubstituted (rhombs) 2,2′-bipyridine (empty) or 1,10-phenathroline (filled), and alkyl (circles) or phenyl (triangles) derivatives.

The KS-LUMO is almost exclusively centred on the diimine ligand both in the gas phase and in DMSO (92–95%, Table S3†). The localization of the KS-LUMO on the N^N ligand is in agreement with what was hypothesized based on the analysis of the electrochemical and spectroscopic data discussed above. Accordingly, the potentials of the two reduction processes $E^{I}_{1/2}$ and $E^{II}_{1/2}$ observed for the complexes are linearly correlated with the KS-eigenvalues calculated for LUMOs of **1–6** in DMSO solution (R^2 = 0.84 and 0.61 for the two reductions; Fig. 10). No significant changes were observed in the composition of the frontier MOs upon varying the solvents considered for the IEF-PCM SCRF calculations in the case of complex **1** (Table S4†).

An analysis of the natural atomic charges[70] calculated on complexes **1–6** shows that a charge separation of about 1.0 and 1.2 *e* exists between the two ligands in the gas phase and in DMSO, respectively (Table S5†). This polarization arises from the partial negative charge carried by the $dtoc^{2-}$ ligand (ranging between −0.54 and −0.71 *e* in the gas phase and between −0.57 and −0.73 *e* in DMSO solution) and the partial positive charge shown by the N^N ligands (in the ranges 0.42–0.46 *e* in the gas phase and 0.57–0.59 *e* in DMSO), the remaining positive charge of the complex being carried by the platinum ion (0.13–0.14 and *e* in DMSO). The calculated charge separation, which confirms what was previously reported for Pt^{II} diimine–dithiolate systems,[34] also shows a small but not negligible dependence on the nature of the solvent (Table S6† for complex **1**).

Time-dependent DFT (TD-DFT) calculations were carried out on complexes **1–6**. Simulated UV–vis absorption spectra of the complexes are in very good agreement with the experimental ones, in particular as far as the solvation calculations are concerned (Tables 4 and S7,† and Fig. 11 for complex **2**). For all complexes, the S0→S2 electronic transition was calculated to be responsible for the lowest energy solvatochromic absorption band observed experimentally in the 410–500 nm region (see above). This transition is mainly assigned to an almost pure (97% for complex **1**, Table 4) monoelectronic excitation between the KS-HOMO−1 and KS-LUMO (KS-MOs 101 and 103, respectively, for complex **1**; Table 4 and Fig. 8), in contrast with the previous DFT calculations reported on complex **6**, where the transitions involving the frontier MOs were calculated to have negligible oscillator strengths.[67] In all complexes, KS-HOMO−1, analogous to KS-HOMO, is a π-in-nature orbital predominantly localized on the sulfur atoms of the $dtoc^{2-}$ ligand, with a significant contribution from the Pt atom (27–28% in DMSO; Fig. 8, 9 and S3† and Table S3†). Thus, given the localization of KS-LUMO described above for complexes **1–6**, the transition could be considered a mixed-metal/ligand-to-ligand CT (MMLL'CT), analogous to most of the [Pt(N^N)(S^S)] complexes reported so far (where it arises from the HOMO→LUMO one-electron excitation).[25]

The CT character of this transition leads to a lowering in the charge separation in the excited state as compared to the GS that accounts for the negative solvatochromism observed.

The KS-LUMO composition also accounts for the linear correlation observed experimentally between the λ_{max} of the corresponding absorption and the reduction potentials $E^{I}_{1/2}$ and $E^{II}_{1/2}$ of complexes **1–6**, and for the dependence of the lowest energy solvatochromic band on the nature of the

Table 4 Main singlet electronic transitions (f > 0.005) calculated for complex **1** in DMSO (IEF-PCM SCRF Model) at the TD-DFT Level. For each transition, the excitation energy E (in eV), the absorption wavelength λ (in nm), the oscillator strength f, and the molecular orbital composition (%) of the excited state functions, along with the fragments where the involved KS-MOs are mainly localized, are reported[a]

Exc. state	E	λ	f	Comp.[a]	%	Assignment
S2	2.553	443.6	0.103	101→103	97	$dtoc^{2-}$(65%) + Pt(27%)→bipy(95%)
S3	3.174	390.6	0.007	102→106	76	$dtoc^{2-}$(73%) + Pt(24%)→$dtoc^{2-}$(43%) + Pt(35%)
S9	3.893	318.5	0.111	102→105	66	$dtoc^{2-}$(73%) + Pt(24%)→bipy(93%)
S10	3.929	315.5	0.008	101→105	79	$dtoc^{2-}$(65%) + Pt(27%)→bipy(93%)
S11	4.385	282.8	0.303	99→103	75	bipy(95%)→bipy(95%)
S13	4.448	278.8	0.043	98→103	90	Pt(53%) + $dtoc^{2-}$(37%)→bipy(95%)
S14	4.515	274.6	0.132	97→103	79	$dtoc^{2-}$(39%) + Pt(38%)→bipy(95%)
S15	4.524	274.1	0.035	100→105	83	Pt(90%)→bipy(93%)

[a] MOs are labelled according to Fig. 8.

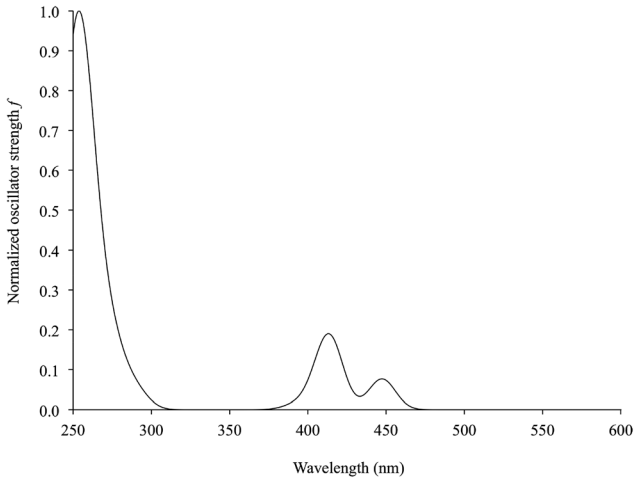

Fig. 11 TD-DFT simulated UV–vis absorption spectrum (230–630 nm) of complex **2** in DMSO (IEF-PCM SCRF model; Table 4).

diimine observed experimentally. Accordingly, the experimental λ_{max} values of the lowest energy solvatochromic absorption can be directly correlated to the eigenvalues of the KS-LUMO calculated for complexes **1–6** (Fig. S4†).

A very good agreement was also found between the experimental and calculated λ_{max} values of the lowest energy absorption in different solvents in the case of complex **1** (R^2 = 0.94; Fig. S5†).[71,72]

As regards complexes **2** and **6** bearing a 1,10-phenanthroline ligand, the solvatochromic absorption observed experimentally in the region 370–540 nm was calculated to derive mainly from the S0→S3 vertical transition (Table S7†). This transition is mainly (73% for complex **2**) due to the KS-HOMO→KS-LUMO+1 monoelectronic excitation (108→110 for complex **2**, Table S7 and Fig. S3†). Also in this case, the excitation can be considered a MMLL'CT, since KS-LUMO+1 is almost exclusively localized on the N^N ligand (99% for complex **2**), thus accounting for its solvatochromism.

Finally, since complexes **1–6** could be exploited as SONLO materials,[41] in analogy with different Pt^{II} complexes,[73] static dipole moments μ and static first hyperpolarizabilities β_{tot} were calculated both in the gas phase and in DMSO (Table 5). The calculated values of β_{tot} (75–136 × 10^{-30} esu in the gas phase) are remarkably lower than those previously calculated for [Pt(N^N)(S^S)] complexes featuring different 1,2-dithiolato ligands (150–650 × 10^{-30} esu in the gas phase),[34] thus confirming the experimental observations reported by Grinstaff and co-workers on the SONLO properties of [Pt(N^N)(S^S)] complexes with S^S = dithiolate *o*-carborane and different 1,2-dithiolates.[42] No significant differences were observed in this case between the hyperpolarizability values calculated in the gas phase and in DMSO, while a clear trend was observed upon varying the N^N ligand. The largest values of β_{tot} were calculated for complexes **5** and **6**, featuring phenyl-substituted diimines, thus confirming that aryl pendants at the N^N ligand could improve the SONLO properties of [Pt(N^N)(S^S)] systems.[34]

Table 5 Static first hyperpolarizability β_{tot} (in a.u. and esu) and static dipole moment μ (in D) calculated for complexes **1–6** in the gas phase and in DMSO (IEF-PCM SCRF model)

	Gas phase			DMSO		
	$\beta_{tot} \times 10^4$ (a.u.)	$\beta_{tot} \times 10^{-30}$ (esu)	$\lvert\mu\rvert$	$\beta_{tot} \times 10^4$ (a.u.)	$\beta_{tot} \times 10^{-30}$ (esu)	$\lvert\mu\rvert$
1	0.87	75	7.43	0.82	71	1.02
2	1.04	90	7.09	0.94	81	9.56
3	0.89	77	7.60	0.76	66	1.00
4	0.99	85	8.26	0.74	64	1.09
5	1.57	136	8.04	1.03	89	1.05
6	1.57	136	8.15	1.07	92	1.05

Conclusions

Five new [Pt(N^N)(S^S)] complexes featuring the 1,2-dithiolato-1,2-*closo*-dicarbadodecaborane ligand ($dtoc^{2-}$) in combination with differently substituted 2,2′-bipyridine and 1,10-phenanthroline ligands were synthesized and characterized by both experimental and theoretical means, and their features were compared to those of the only previously reported complex of the same type (**6**). The very first structural information on [Pt(N^N)(dtoc)] complexes were also obtained by single crystal X-ray diffraction.

As already observed for different Pt^{II} diimine–dithiolate complexes, solvatochromic absorptions are displayed in the visible region of the complexes' spectra, and in particular a single broad absorption was observed in the case of the complexes featuring a 2,2′-bipyridine derivative (λ_{max} = 420–440 nm in DMSO). Based on TD-DFT calculations, the broad absorption was attributed to the HOMO−1/LUMO electronic excitation, whose MMLL'CT character accounts for its solvatochromism. On the other hand, two different bands were shown in the case of complexes bearing 1,10-phenanthroline derivatives (λ_{max} = 427–441 nm in DMSO), both assigned to excitations having a MMLL'CT character as well. The DFT calculations reported in this work thus allowed for the first persuasive interpretation of the peculiar spectroscopic features of [Pt(N^N)(dtoc)] complexes, in particular those containing the 1,10-phenanthroline moiety.

In the title complexes, the electron-withdrawing effect of the $dtoc^{2-}$ ligand determines a remarkable stabilization of the HOMOs and HOMO−1s with respect to [Pt(N^N)(S^S)] systems bearing different sulfur ligands. Thus, no oxidation processes were observed by CV in DMSO solution within the explored range of potentials (−2.5–1.5 V *vs.* Fc^+/Fc). As a consequence, the energy gap between HOMO/HOMO−1 and LUMO is significantly increased with respect to other [Pt(N^N)(S^S)] complexes, thus shifting the typical solvatochromic absorption to higher energies.

It is worth underlining that the peculiar electronic structure of [Pt(N^N)(S^S)] complexes allows the fine-tuning of the energy of their frontier orbitals by a proper choice of the ligands, and hence the tailoring of both the electrochemical stability of the neutral complexes and the energy of the solvatochromic visible absorption. In this context:

(1) Donor S^S ligands raise HOMOs eigenvalues, while electron-withdrawing dithiolates, such as $dtoc^{2-}$, exert the opposite effect.

(2) Diimines with donor (alkyl) substituents feature the LUMO at higher energy as compared to phenyl-substituted ones.

(3) As a consequence, on passing from complexes featuring a donor dithiolate and a phenyl-substituted diimine, such as [Pt(Ph_2bipy)(Me-dmet)], to complexes featuring electron-withdrawing dithiolates and alkyl-substituted diimines, such as [Pt(Me_2bipy)(dtoc)], the wavelength of the solvatochromic band can be varied by more than 150 nm in DMSO (λ_{max} = 437 and 602 nm for [Pt(Me_2bipy)(dtoc)] and [Pt(Ph_2bipy)-(Me-dmet)], respectively).

Finally, the calculated β_{tot} values show that [Pt(N^N)(dtoc)] complexes have a less pronounced SONLO behaviour in comparison with [Pt(N^N)(S^S)] systems bearing 1,2-dithiolene ligands. The static β_{tot} values reported in this work are in agreement with the trend previously observed with regard to the influence of the N^N ligand on the hyperpolarizability values, which showed that the presence of phenyl substituents increases β_{tot} values.

The insight into the electrochemical and linear and nonlinear spectroscopic features of [Pt(N^N)(dtoc)] complexes given in the present work represents therefore a significant step forward in the understanding of the electronic features of this class of compounds, and opens the way to their employment in devices of interest in optical processing.

Experimental section

Chemicals

2,2′-Bipyridine, 1,10-phenanthroline and derivatives, $K_2[PtCl_4]$, *n*-butyllithium (*n*-BuLi) were obtained from commercial sources. The solvents for the syntheses were of reagent grade. THF was freshly distilled on $LiAlH_4$ before use.

Synthesis of complexes

Platinum dichlorodiimine complexes $[PtCl_2(N^N)]$[44,45] and 1,2-dithiol-1,2-*closo*-dicarbadodecarborane[40] were synthesized according to published procedures. The complex [Pt(Ph_2phen)-(dtoc)] (**6**) was synthesized through a modification of the procedure reported in the literature.[41] Compounds **1–5** were all synthesized according to a similar procedure, described here in detail for complex **1**. The details of the characterization of complexes **2–5** are available as ESI.†

[Pt(bipy)(dtoc)] (1). To a solution of 1,2-dithiolato-1,2-*closo*-dicarbadodecarborane (0.10 g, 0.48 mmol) in 5 mL of dry THF a two-fold excess (0.96 mmol) of *n*-BuLi in hexane solution was added dropwise under a nitrogen atmosphere at 0° C, and the reaction mixture was stirred for 2 hours at the same temperature. An equimolar suspension of $[PtCl_2(bipy)]$ (0.20 g, 0.48 mmol) in 20 mL of the same solvent was then added dropwise, and the system was left under magnetic stirring and under N_2 at room temperature for one week. The resulting orange precipitate was collected by filtration and washed with water. X-ray quality crystals were obtained by slow infusion of petroleum ether into a dichloromethane solution of the complex. Yield: 0.15 g (58%); m.p. >240 °C; FTIR: $\tilde{\nu}$ = 414 (s), 470 (w), 674 (w), 680 (w), 719 (s), 723 (s), 755 (vs), 794 (w), 868 (s), 919 (w), 929 (w), 972 (m), 1024 (w), 1071 (m), 1110 (w), 1126 (w), 1163 (m), 1178 (w), 1205 (vw), 1243 (w), 1319 (m), 1384 (w), 1432 (m), 1448 (s), 1471 (s), 1560 (w), 1605 (s), 1944 (vw), 1979 (vw), 2346 (vw), 2557 (s), 2580 (s), 2626 (w), 3027 (vw), 3046 (vw), 3077 (vw), 3116 (vw) cm^{-1}; UV-vis-NIR (CH_2Cl_2): λ (ε) = 230 (24 500), 295 (19 500), 303 (sh, 18 700), 447 nm (6300 M^{-1} cm^{-1}); $^{13}C\{^1H\}$ NMR (DMF): δ = 155.0, 148.0, 140.0, 128.5, 124.3 (C_{aryl}), 85.7 ($C_{cluster}$); ^{11}B NMR (DMF): δ = −2.6 (2B, broad singlet), −7.7 (6B, ^1J(B,H) = 125), −10.7 (2B, ^1J(B,H) = 128); elemental analysis calcd (%) for $C_{12}H_{18}N_2S_2B_{10}Pt$: C 25.84, H 3.28, N 5.02; found: C 26.01, H 3.31, N 4.93; CV (DMSO): $E_{1/2}$ *vs.* Fc^+/Fc (scan rate = 100 mV s^{-1}) = −1.593, −2.251 V.

Characterization

Microanalyses were performed by using a Perkin-Elmer 240 B microanalyser. Infrared spectra were recorded on a Thermo-Nicolet 5700 spectrometer at room temperature: KBr pellets with a KBr beam-splitter and KBr windows (4000–400 cm^{-1}, resolution 4 cm^{-1}) were used. The ^{1}H-NMR (300.13 MHz), $^{13}C\{^1H\}$-NMR (75.47 MHz) and ^{11}B-NMR (96.29 MHz) spectra were recorded on a Bruker ARX 300WB spectrometer. Chemical shift values for ^{1}H-NMR spectra were referenced to an internal standard of $SiMe_4$ in deuterated solvents. The $^{13}C\{^1H\}$-NMR spectra of slightly soluble compounds were dissolved in DMF and spectra run in a double tube containing acetone-d_6. Chemical shift values for ^{11}B-NMR spectra were referenced relative to external $BF_3{\cdot}OEt_2$. Chemical shifts are reported in units of parts per million downfield from the reference, and all coupling constants are reported in hertz. Absorption spectra were recorded on solutions of the investigated complexes in spectrophotometric grade solvents at 298 K in a quartz cell of 10.00 mm optical path using a Thermo Evolution 300 (190–1100 nm) spectrophotometer. Cyclic voltammetry measurements (scan rate 10–1000 mV s^{-1}) were performed in dry DMSO in a Metrohm voltammetric cell, with a combined working and counter platinum electrode and a standard Ag/AgCl reference electrode using a Metrohm Autolab PGSTAT 10 potentiostat ($C \approx 1.5 \times 10^{-3}$ M; supporting the electrolyte $[NBu_4][PF_6]$ 0.10 M): reported data are referred to the Fc^+/Fc reversible couple. The DMSO solutions were deaerated with analytical grade nitrogen at the start of each experiment to prevent oxygen interference. All experiments were performed at room temperature.

X-ray crystallography

Single crystal X-ray diffraction data were collected at 120(2) K by combined Φ and Ω scans on a Bruker Nonius KappaCCD area detector situated at the window of a rotating anode (graphite $Mo_{K\alpha}$ radiation, λ = 0.71073 Å). The structures were solved by direct methods with SHELXS-97 and refined on F^2 by using SHELXL-97.[74] Complete crystallographic data have been deposited at the Cambridge Crystallographic Data Centre, CCDC 1010434 (complex **1**) and 1010435 (complex **4**).

DFT calculations

Theoretical calculations were performed at the DFT level[57] with the Gaussian 09 suite of programs (rev. A.02)[75] on a E4 workstation equipped with four quad-core AMD Opteron processors and 16 Gb of RAM, running the 64 bit version of the Ubuntu 12.04 Linux operating system. The PBE0 (PBE1PBE) hybrid functional was adopted,[58] and Schäfer, Horn, and Ahlrichs double-ζ plus polarization all-electron basis sets[59] were used for C, H, N, B, and S, whereas CRENBL BS[60] with relativistic effective core potentials (RECPs)[61,62] was chosen for the heavier Pt species. The tight SCF convergence criterion (*SCF = tight* keyword) and fine numerical integration grids [*Integral-(FineGrid)* keyword] were used. The nature of the minima of each optimized structure was verified by harmonic frequency calculations (*freq = raman* keyword). Natural[70] and Mulliken[76] atomic charges were calculated at the optimized geometries at the same level of theory, and electronic transition energies and oscillator strength values were calculated at the TD-DFT level (100 states). The electronic spectra were simulated by a convolution of Gaussian functions centered at the calculated excitation energies. Solvation calculations were also carried out in the presence of a set of different solvents (CH_2Cl_2, $CHCl_3$, CH_3CN, acetone, THF, DMF, DMSO, and toluene), implicitly taken into account by the polarizable continuum model in its integral equation formalism variant (IEF-PCM).[64] The total static second-order (quadratic) hyperpolarizability (the first hyperpolarizability)[77] β_{tot} was calculated as described by Mendes *et al*.[78] from the relation:

$$\beta_{tot} = \sqrt{\beta_x^2 + \beta_y^2 + \beta_z^2}$$

where each static component β_i ($i = x, y, z$) is obtained from the equation:

$$\beta_i = \beta_{iii} + \frac{1}{3}\sum_{i<>j}(\beta_{ijj} + \beta_{jij} + \beta_{jji})$$

By using Kleinman symmetry relationships,[79] the final equation was obtained:

$$\beta_{tot} = \sqrt{(\beta_{xxx} + \beta_{xyy} + \beta_{xzz})^2 + (\beta_{yyy} + \beta_{yzz} + \beta_{yxx})^2 + (\beta_{zzz} + \beta_{zxx} + \beta_{zyy})^2}$$

The programs Gaussview 5.0[80] and Molden 5.0[81] were used to investigate the charge distributions and molecular orbital shapes. The software GaussSum 2.1[82] was used to calculate the molecular orbital contributions (MOC) from groups of atoms, along with the contribution of singly excited configurations to each electronic transition, and to generate all the necessary data to simulate absorption spectra.

Acknowledgements

The Università degli Studi di Cagliari, the Ministero dell'Istruzione, dell'Università e della Ricerca (MIUR, PRIN 2009Z9ASCA) and the Regione Autonoma della Sardegna are acknowledged for financial support. M. Arca thanks the Consorzio interuniversitario per le Applicazioni di Supercalcolo Per Università e Ricerca (CASPUR) for providing computational resources within the framework of HPC grants 2012. This work was supported by Generalitat de Catalunya (2009/SGR/00279), European Union (FP7-OCEAN-2013-614168) and COST Action CM1302. A.-D. Musteti thanks the Spanish Ministerio de Educación for a FPU grant (AP2008-02290). The Engineering and Physical Sciences Research Council is acknowledged for funding the UK National Crystallography Service. A.-D. Musteti is enrolled in the UAB PhD program.

Notes and references

1 T. R. Miller and I. G. Dance, *J. Am. Chem. Soc.*, 1973, **95**, 6970–6979.
2 C.-T. Chen, S. Y. Liao, K.-J. Lin and L.-L. Lai, *Adv. Mater.*, 1998, **3**, 334–338.
3 H.-B. Zhao, Y.-Q. Qiu, C.-G. Liu, S.-L. Sun, Y. Liu and R.-S. Wang, *J. Organomet. Chem.*, 2010, **695**, 2251–2257.
4 E. A. M. Geary, N. Hirata, J. Clifford, J. R. Durrant, S. Parsons, A. Dawson, L. J. Yellowlees and N. Robertson, *Dalton Trans.*, 2003, 3757–3762.
5 A. Islam, H. Sugihara, K. Hara, L. P. Singh, R. Katoh, M. Yanagida, Y. Takahashi, S. Murata and H. Arakawa, *Inorg. Chem.*, 2001, **40**, 5371–5380.
6 C. L. Linfoot, P. Richardson, K. L. McCall, J. R. Durrant, A. Morandeira and N. Robertson, *Sol. Energy*, 2011, **85**, 1195–1203.
7 A. Islam, H. Sugihara, K. Hara, L. P. Singh, R. Katoh, M. Yanagida, Y. Takahashi, S. Murata and H. Arakawa, *New J. Chem.*, 2000, **24**, 343–345.
8 E. A. M. Geary, K. L. McCall, A. Turner, P. R. Murray, E. J. L. McInnes, L. A. Jack, L. J. Yellowlees and N. Robertson, *Dalton Trans.*, 2008, 3701–3708.
9 M. Hissler, J. E. McGarrah, W. B. Connick, D. K. Geiger, S. D. Cummings and R. Eisenberg, *Coord. Chem. Rev.*, 2000, **208**, 115–137.
10 J. Zhang, P. Du, J. Schneider, P. Jarosz and R. Eisenberg, *J. Am. Chem. Soc.*, 2007, **129**, 7726–7727.
11 C. A. Mitsopoulou, C. E. Dagas and C. Makedonas, *Inorg. Chim. Acta*, 2008, **361**, 1973–1982.
12 C. A. Mitsopoulou, C. E. Dagas and C. Makedonas, *J. Inorg. Biochem.*, 2008, **102**, 77–86.

13 K. Kubo, M. Nakano, H. Tamura and G. Matsubayashi, *Inorg. Chim. Acta*, 2002, **336**, 120–124.
14 B. W. Smucker, J. M. Hudson, M. A. Omary and K. R. Dunbar, *Inorg. Chem.*, 2003, **42**, 4714–4723.
15 Y. Ji, R. Zhang, X.-B. Du, J.-L. Zuo and X.-Z. You, *Dalton Trans.*, 2008, 2578–2582.
16 E. A. M. Geary, L. J. Yellowlees, L. A. Jack, I. D. H. Oswald, S. Parsons, N. Hirata, J. R. Durrant and N. Robertson, *Inorg. Chem.*, 2005, **44**, 242–250.
17 S. D. Cummings, L.-T. Cheng and R. Eisemberg, *Chem. Mater.*, 1997, **9**, 440–450.
18 J. A. Zuleta, J. M. Bevilacqua, J. M. Rehm and R. Eisenberg, *Inorg. Chem.*, 1992, **31**, 1332–1337.
19 J. M. Bevilacqua and R. Eisenberg, *Inorg. Chem.*, 1994, **33**, 2913–2923.
20 S. D. Cummings and R. Eisenberg, *J. Am. Chem. Soc.*, 1996, **118**, 1949–1960.
21 C.-T. Chen, S.-Y. Liao, K.-J. Lin, C.-H. Chen and T.-Y. J. Lin, *Inorg. Chem.*, 1999, **38**, 2734–2741.
22 C. Makedonas and C. A. Mitsopoulou, *Inorg. Chim. Acta*, 2007, **360**, 3997–4009.
23 C. Makedonas, C. A. Mitsopoulou, F. J. Lahoz and A. I. Balana, *Inorg. Chem.*, 2003, **42**, 8853–8865.
24 J. A. Zuleta, J. M. Bevilacqua, D. M. Proserpio, P. D. Harvey and R. Eisenberg, *Inorg. Chem.*, 1992, **31**, 2396–2404.
25 C. A. Mitsopoulou, *Coord. Chem. Rev.*, 2010, **254**, 1448–1456.
26 J. A. Zuleta, M. S. Burberry and R. Eisenberg, *Coord. Chem. Rev.*, 1990, **97**, 47–64.
27 J. A. Zuleta, J. M. Bevilacqua and R. Eisenberg, *Coord. Chem. Rev.*, 1991, **111**, 237–248.
28 T. M. Cocker and R. E. Bachman, *Inorg. Chem.*, 2001, **40**, 1550–1556.
29 W. Paw, S. D. Cummings, M. A. Mansour, W. B. Connick, D. K. Geiger and R. Eisenberg, *Coord. Chem. Rev.*, 1998, **171**, 125–150.
30 L. Ambrosio, M. C. Aragoni, M. Arca, F. A. Devillanova, M. B. Hursthouse, S. L. Huth, F. Isaia, V. Lippolis, A. Mancini and A. Pintus, *Chem. – Asian J.*, 2010, **5**, 1395–1406.
31 M. C. Aragoni, M. Arca, F. A. Devillanova, F. Isaia, V. Lippolis and A. Pintus, *Chem. – Asian J.*, 2011, **6**, 198–208.
32 M. C. Aragoni, M. Arca, F. A. Devillanova, F. Isaia, V. Lippolis, A. Mancini, L. Pala, A. M. Z. Slawin and J. D. Woollins, *Inorg. Chem.*, 2005, **44**, 9610–9612.
33 S. Eid, M. Formigué, T. Roisnel and D. Lorcy, *Inorg. Chem.*, 2007, **46**, 10647–10654.
34 A. Pintus, M. C. Aragoni, N. Bellec, F. A. Devillanova, D. Lorcy, F. Isaia, V. Lippolis, R. A. M. Randall, T. Roisnel, A. M. Z. Salwin, J. D. Woollins and M. Arca, *Eur. J. Inorg. Chem.*, 2012, 3577–3594.
35 (*a*) R. N. Grimes, *Carboranes*, Academic Press, London, 2nd edn, 2011; (*b*) F. Teixidor and C. Viñas, in *Science of Synthesis*, ed. D. E. Kauffmann and D. S. Matteson, Thieme, Stuttgart, 2005, vol. 6, p. 1235.
36 F. Teixidor, C. Viñas, A. Demonceau and R. Nuñez, *Pure Appl. Chem.*, 2003, **75**, 1305–1313.
37 (*a*) F. Teixidor, R. Núñez, C. Viñas, R. Sillanpää and R. Kivekäs, *Angew. Chem., Int. Ed.*, 2000, **39**, 4460–4462; (*b*) R. Núñez, P. Farràs, F. Teixidor, C. Viñas, R. Sillanpää and R. Kivekäs, *Angew. Chem., Int. Ed.*, 2006, **45**, 1292–1294.
38 L. Schwartz, L. Eriksson, R. Lomoth, F. Teixidor, C. Viñas and S. Ott, *Dalton Trans.*, 2008, 2379–2381.
39 F. Teixidor, G. Barberà, A. Vaca, R. Kivekäs, R. Sillanpää, J. Oliva and C. Viñas, *J. Am. Chem. Soc.*, 2005, **127**, 10158–10159.
40 H. D. Smith, C. O. Obenland and S. Papetti, *Inorg. Chem.*, 1966, **5**, 1013–1015.
41 K. Base and M. W. Grinstaff, *Inorg. Chem.*, 1998, **37**, 1432–1433.
42 K. Base, M. T. Tierney, A. Fort, J. Muller and M. W. Grinstaff, *Inorg. Chem.*, 1999, **38**, 287–289.
43 J. A. Weinstein, M. T. Tierney, E. S. Davies, K. Base, A. A. Robeiro and M. W. Grinstaff, *Inorg. Chem.*, 2006, **45**, 4544–4555.
44 G. T. Morgan and F. H. Burstall, *J. Chem. Soc.*, 1934, 965–971.
45 J. V. Rund, *Inorg. Chem.*, 1974, **13**, 738–740.
46 J. A. Todd, D. Caiazza, E. R. T. Tiekink and L. M. Rendina, *Inorg. Chim. Acta*, 2003, **352**, 208–212.
47 An examination of the CDS (v. 5.33, updated Feb. 2014) provided to date 37 authentic examples of monomeric [Pt(N^N)(S^S)] complexes.
48 81 complexes featuring the 1,2-dithiolate-*closo*-1,2-dicarbadodecarborane acting as a bidentate ligand toward a single metal ion were found in the CDS (v. 5.33, updated Feb. 2014).
49 R. Coult, M. A. Fox, W. R. Gill and K. Wade, *Polyhedron*, 1992, **11**, 2717–2721.
50 The S–Pt–S angles show values similar to those found for the 1,2-dimercapto-*o*-carborane Pt complexes [Pt(dtoc)-$(PMe_2Ph)_2$] and [Pt(dtoc)$(PMePh_2)_2$], recently reported by: M. K. Pal, V. K. Jain, A. P. Wadawale, S. A. Glazun, Z. A. Starikova and V. I. Bregadze, *J. Organomet. Chem.*, 2012, **696**, 4257–4263.
51 A search of the Cambridge Crystallographic Database shows that the contacts' distances fall in the range of similar platinum–$C_{2,2\text{-bipy}}$ contacts in 2,2′-bipyridine Pt complexes. See for example: D. E. Janzen and K. R. Mann, *J. Chem. Crystallogr.*, 2013, **43**, 292–298; J. Ni, X. Zhang, N. Qiu, Y.-H. Wu, L.-Y. Zhang, J. Zhang and Z.-N. Chen, *Inorg. Chem.*, 2011, **50**, 9090–9096.
52 C. E. Keefer, R. D. Bereman, S. T. Purrington, B. W. Knight and P. D. Boyle, *Inorg. Chem.*, 1999, **38**, 2294–2302.
53 Solvent molecules can freely move up and down the voids hence the type of alkane cannot be unambiguously confirmed by X-ray diffraction analysis. The electron density in the voids was smoothed using the SQUEEZE module in Platon.

54 $E^{I}_{1/2}$ = −1.608, −1.620, −1.740, −1.692, −1.563, and −1.561 V *vs*. Fc^{+}/Fc for complexes [Pt(N^N)(Me-dmet)] featuring N^N = bipy, phen, Me_2bipy, *t*Bu_2bipy, Ph_2bipy, and Ph_2phen, respectively. See ref. 34.
55 P. S. Braterman, J.-I. Song, F. M. Wimmer, S. Wimmer, W. Kaim, A. Klein and R. D. Peacock, *Inorg. Chem.*, 1992, **31**, 5084–5088.
56 The reduction step was recorded in DMF solution at −2.071, −2.12, −2.082, and −2.105 V for [Pt(bipy)$(py)_2$], [Pt(bipy)$(Me_2$N-py)], [Pt(bipy)(en)], and [Pt(phen)$(py)_2$].
57 W. Koch and M. C. Holthausen, *A Chemist's Guide to Density Functional Theory*, Wiley-VCH, Weinheim, Germany, 2nd edn, 2002.
58 C. Adamo and V. Barone, *J. Chem. Phys.*, 1999, **110**, 6158–6170.
59 A. Schäfer, H. Horn and R. Ahlrichs, *J. Chem. Phys.*, 1992, **97**, 2571–2577.
60 W. C. Ermler, R. B. Ross and P. A. Christiansen, *Int. J. Quantum. Chem.*, 1991, **40**, 829–846.
61 T. H. Dunning Jr. and P. J. Hay, in *Methods of Electronic Structure, Theory*, ed. H. F. Schaefer III, Plenum Press, New York, 1977, vol. 2.
62 J. V. Ortiz, P. J. Hay and R. L. Martin, *J. Am. Chem. Soc.*, 1992, **114**, 2736–2737.
63 B. A. Hess, *Relativistic Effects in Heavy Element Chemistry and Physics*, Wiley-VCH, Weinheim, 2003.
64 J. Tomasi, B. Mennucci and R. Cammi, *Chem. Rev.*, 2005, **105**, 2999–3094.
65 In particular, the optimised C(1)–C(2) bond distances vary within 0.002 Å along the series of the solvents considered in this work (Table S2†), thus factoring out a direct relationship between the structural features of the 1,2-dithiolates and the observed solvatochromic behaviour, reported recently in the case of different fluorescent *o*-carborane derivatives; see: A. Ferrer-Ugalde, A. González-Campo, C. Viñas, J. Rodríguez-Romero, R. Santillan, N. Farfán, R. Sillampaä, A. Sousa-Pedrares, R. Núñes and F. Teixidor, *Chem. – Eur. J.*, 2014, DOI: 10.1002/chem.201402396.
66 Notably, the MO composition calculated here is different from the results previously reported for **6** in ref. 67, where – in contrast with experimental spectroscopic and electrochemical measurements – both the HOMO and the LUMO were reported to be centered on the diimine.
67 X. Liu, Y. Qiu, H. Chen, N. Li, S. Sun and Z. Su, *Sci. China, Ser. B: Chem.*, 2009, **52**, 144–152.
68 KS-HOMO eigenvalues calculated in the gas phase for complexes **1–6**: −5.73, −5.69, −5.58, −5.52, −5.59, −5.56 eV, respectively.
69 KS-HOMO eigenvalues calculated in the gas phase: −4.49, −4.43, −4.33, −4.49, −4.39, and −4.34 eV for N^N = bipy, phen, Me_2bipy, *t*Bu_2bipy, Ph_2bipy, and Ph_2phen, respectively. See ref. 34.
70 A. E. Reed, R. B. Weinstock and F. Weinhold, *J. Chem. Phys.*, 1985, **83**, 735–746.
71 Calculated λ_{max} values (nm) of the S0→S2 vertical transition for complexes **1–6** in DMSO (IEF-PCM SCRF model): 444, 444, 437, 425, 459, and 459 nm, respectively.
72 Calculated λ_{max} values: CH_2Cl_2 462, $CHCl_3$ 481, CH_3CN 444, acetone 449, DMF 445, THF 466, toluene 519 nm.
73 (*a*) A. Colombo, C. Dragonetti, D. Marinotto, S. Righetto, D. Roberto, S. Tavazzi, M. Escadeillas, V. Guerchais, H. Le Bozec, A. Boucekkine and C. Latouche, *Organomet. Chem.*, 2013, **32**, 3890–3894; (*b*) A. Valore, A. Colombo, C. Dragonetti, S. Righetto, D. Roberto, R. Ugo, F. De Angelis and S. Fantacci, *Chem. Commun.*, 2010, **46**, 414–2416; (*c*) S. De Bella, C. Dragonetti, M. Pizzotti, D. Roberto, F. Tessore and R. Ugo, *Top. Organomet. Chem.*, 2010, **28**, 1–55.
74 G. M. Sheldrick, *Acta Crystallogr., Sect. D: Biol. Crystallogr.*, 2008, **64**, 112–122.
75 M. J. Frisch, G. W. Trucks, H. B. Schlegel, G. E. Scuseria, M. A. Robb, J. R. Cheeseman, G. Scalmani, V. Barone, B. Mennucci, G. A. Petersson, H. Nakatsuji, M. Caricato, X. Li, H. P. Hratchian, A. F. Izmaylov, J. Bloino, G. Zheng, J. L. Sonnenberg, M. Hada, M. Ehara, K. Toyota, R. Fukuda, J. Hasegawa, M. Ishida, T. Nakajima, Y. Honda, O. Kitao, H. Nakai, T. Vreven, J. A. Montgomery Jr., J. E. Peralta, F. Ogliaro, M. Bearpark, J. J. Heyd, E. Brothers, K. N. Kudin, V. N. Staroverov, R. Kobayashi, J. Normand, K. Raghavachari, A. Rendell, J. C. Burant, S. S. Iyengar, J. Tomasi, M. Cossi, N. Rega, J. M. Millam, M. Klene, J. E. Knox, J. B. Cross, V. Bakken, C. Adamo, J. Jaramillo, R. Gomperts, R. E. Stratmann, O. Yazyev, A. J. Austin, R. Cammi, C. Pomelli, J. W. Ochterski, R. L. Martin, K. Morokuma, V. G. Zakrzewski, G. A. Voth, P. Salvador, J. J. Dannenberg, S. Dapprich, A. D. Daniels, O. Farkas, J. B. Foresman, J. V. Ortiz, J. Cioslowski and D. J. Fox, *Gaussian 09, Revision A.02*, Gaussian, Inc., Wallingford CT, 2009.
76 R. S. Mulliken, *J. Chem. Phys.*, 1955, **23**, 1833–1840.
77 M. P. Cifuentes and M. G. Humphrey, *J. Organomet. Chem.*, 2004, 3968–3981.
78 P. J. Mendes, A. J. P. Carvalho and J. P. P. Ramalho, *J. Mol. Struct. (THEOCHEM)*, 2009, **900**, 110–117.
79 D. A. Kleinman, *Phys. Rev.*, 1962, **126**, 1977–1979.
80 R. Dennington, T. Keith and J. Millam, *GaussView, Version 5*, Semichem Inc., Shawnee Mission KS, 2009.
81 G. Schaftenaar and J. H. Noordik, *J. Comput.-Aided Mol. Des.*, 2000, **14**, 123–134.
82 N. M. O'Boyle, A. L. Tenderholt and K. M. Langner, *J. Comput. Chem.*, 2008, **29**, 839–845.

